

Determination of polarized parton distribution functions with recent data on polarization asymmetries

M. Hirai,^{1,*} S. Kumano,^{1,2,†} and N. Saito^{3,‡}

(Asymmetry Analysis Collaboration)

¹*Institute of Particle and Nuclear Studies*

High Energy Accelerator Research Organization (KEK)

1-1, Ooho, Tsukuba, Ibaraki, 305-0801, Japan

²*Department of Particle and Nuclear Studies*

The Graduate University for Advanced Studies

1-1, Ooho, Tsukuba, Ibaraki, 305-0801, Japan

³*Department of Physics, Kyoto University, Kyoto, 606-8502, Japan*

(Dated: March 25, 2006)

Global analysis has been performed within the next-to-leading order in Quantum Chromodynamics (QCD) to determine polarized parton distributions with new experimental data in spin asymmetries. The new data set includes JLab, HERMES, and COMPASS measurements on spin asymmetry A_1 for the neutron and deuteron in lepton scattering. Our new analysis also utilizes the double-spin asymmetry for π^0 production in polarized pp collisions, $A_{LL}^{\pi^0}$, measured by the PHENIX collaboration. Because of these new data, uncertainties of the polarized PDFs are reduced. In particular, the JLab, HERMES, and COMPASS measurements are valuable for determining $\Delta d_v(x)$ at large x and $\Delta \bar{q}(x)$ at $x \sim 0.1$. The PHENIX π^0 data significantly reduce the uncertainty of $\Delta g(x)$. Furthermore, we discuss a possible constraint on $\Delta g(x)$ at large x by using the HERMES data on g_1^d in comparison with the COMPASS ones at $x \sim 0.05$.

PACS numbers: 13.60.Hb, 13.88.+e

I. INTRODUCTION

The nucleon spin structure has been investigated mainly by polarized lepton-nucleon scattering experiments. After many years of theoretical and experimental efforts, our knowledge on the spin structure of the nucleon is much improved especially in the valence-quark sector. However, we still miss a decent measurement of orbital angular momenta, transversity distributions, and helicity distributions of sea-quarks and gluons in the proton. In particular, the polarized gluon distribution has large uncertainty. For example, the AAC analysis indicated that the first moment of $\Delta g(x)$ is $\Delta g = 0.50 \pm 1.27$ at $Q^2=1 \text{ GeV}^2$ [1, 2]. This represents the largest ambiguity in understanding the longitudinal spin-structure of the proton; Δg , the gluon spin contribution to the proton can be either positive or negative.

Fortunately, various experiments started to produce data which are sensitive to the gluon polarization. First, there were reports on $\Delta g(x)/g(x)$ from HERMES [3], SMC (Spin Muon Collaboration) [4], and COMPASS [5] collaborations by using high- p_T hadron production measurements in polarized lepton-nucleon scattering. There are also preliminary results [6] from the COMPASS by using the data for charmed-meson and high- p_T -hadron productions. Second, the RHIC (Relativistic Heavy Ion Col-

lider) Spin experiments started to produce data which could constrain the gluon polarization. They are spin-asymmetry measurements in pion [7, 8] and jet [9] productions in polarized pp reactions by PHENIX and STAR collaborations, respectively. Because of these new data, we expect much improved determination of the polarized gluon distribution.

There are also new measurements on the spin asymmetry A_1 in lepton-nucleon scattering by JLab (Thomas Jefferson National Accelerator Facility) Hall A [10], HERMES [11], and COMPASS [12] collaborations in addition to the data set used in our previous analysis [2]. These data should be useful for a better determination of quark and anti-quark distributions, and they may also provide a constraint on the gluon polarization through scaling violation. In addition, the PHENIX π^0 data can be included in the analysis for a better determination of the polarized gluon distribution.

The major updates from the previous analysis [2] is the addition of these new data. Using these reaction data, we determine the polarized parton distribution functions (PDFs). We discuss analysis results by demonstrating the importance of each experiment. In particular, new points are the discussions on:

1. impact of the JLab, HERMES, and COMPASS data on the determination of $\Delta q(x)$ and $\Delta \bar{q}(x)$,
2. impact of PHENIX data on the determination of $\Delta g(x)$,
3. constraint on $\Delta g(x)$ from the differences between HERMES and COMPASS data on g_1^d at $x \sim 0.05$.

*E-mail: mhirai@post.kek.jp

†E-mail: shunzo.kumano@kek.jp

‡E-mail: saito@nh.scphys.kyoto-u.ac.jp

This paper is organized as follows. In Sec. II, our analysis method is described for determining the polarized PDFs. Analysis results are explained in Sec. III. The parametrization results are compared with recent spin asymmetry data, the optimum polarized PDFs are shown, and they are discussed in comparison with other PDFs. Then, details of the polarized gluon distribution is discussed in Sec. IV. The results are summarized in Sec. V.

II. ANALYSIS METHOD

Spin-asymmetry data are analyzed to obtain the polarized PDFs. In lepton-nucleon deep inelastic scattering (DIS), the spin asymmetry A_1 is given by unpolarized structure function F_2 , longitudinal-transverse structure function ratio R , and polarized structure function g_1 [13]:

$$A_1(x, Q^2) = \frac{g_1(x, Q^2)}{F_2(x, Q^2)} 2x [1 + R(x, Q^2)], \quad (1)$$

where Q^2 is given by the momentum transfer q as $Q^2 = -q^2$, and x is the Bjorken scaling variable defined by $x = Q^2/(2p \cdot q)$ with the nucleon momentum p . The structure function g_1 is expressed [14]:

$$g_1(x, Q^2) = \frac{1}{2} \sum_{i=1}^{n_f} e_i^2 \left\{ \Delta C_q(x, \alpha_s) \otimes [\Delta q_i(x, Q^2) + \Delta \bar{q}_i(x, Q^2)] + \Delta C_g(x, \alpha_s) \otimes \Delta g(x, Q^2) \right\}, \quad (2)$$

where ΔC_q and ΔC_g are polarized coefficient functions, and Δq_i , $\Delta \bar{q}_i$, and Δg are polarized quark, antiquark, and gluon distribution functions, respectively. The symbol \otimes denotes the convolution integral:

$$f(x) \otimes g(x) = \int_x^1 \frac{dz}{z} f(z) g\left(\frac{x}{z}\right). \quad (3)$$

In the similar way, the structure function F_2 is expressed in terms of unpolarized PDFs and coefficient functions. The structure functions are calculated in the next-to-leading-order (NLO) of the running coupling constant α_s , and the modified minimal subtraction ($\overline{\text{MS}}$) scheme is used.

The longitudinal double spin asymmetry for pion production in polarized pp reaction is given by [7, 8]

$$A_{LL}^{\pi^0} = \frac{[d\sigma_{++} - d\sigma_{+-}]/dp_T}{[d\sigma_{++} + d\sigma_{+-}]/dp_T} = \frac{d\Delta\sigma/dp_T}{d\sigma/dp_T}, \quad (4)$$

where p_T is the transverse momentum of the pion, and $\sigma_{h_1 h_2}$ is the cross section with the proton helicities h_1 and h_2 . The cross sections $\Delta\sigma$ and σ are defined by $\Delta\sigma = (\sigma_{++} - \sigma_{+-})/2$ and $\sigma = (\sigma_{++} + \sigma_{+-})/2$. The

polarized cross sections are expressed in terms of the polarized PDFs Δf and fragmentation functions $D_c^{\pi^0}$ [15]:

$$\frac{d\Delta\sigma}{dp_T} = \sum_{a,b,c} \int_{\eta_{\min}}^{\eta_{\max}} d\eta \int_{x_a^{\min}}^1 dx_a \Delta f_a(x_a) \times \int_{x_b^{\min}}^1 dx_b \Delta f_b(x_b) \frac{\partial(\hat{t}, z_c)}{\partial(p_T, \eta)} \frac{d\Delta\hat{\sigma}_{a+b \rightarrow c+X}}{d\hat{t}} D_c^{\pi}(z_c), \quad (5)$$

where $\partial(\hat{t}, z_c)/\partial(p_T, \eta)$ is the Jacobian. The cross section $d\Delta\hat{\sigma}_{a+b \rightarrow c+X}/d\hat{t}$ is for the parton-level subprocess $a + b \rightarrow c + X$, and its expression is, for example, found in Ref. [16]. The variables x_a and x_b are momentum fractions for the partons a and b , respectively, and z_c is the momentum fraction given by $z_c = p_\pi/p_c$ with the pion momentum p_π and the parton momentum p_c . The pseudorapidity η and \hat{t} are defined by

$$\eta = -\ln \left[\tan \left(\frac{\theta_\pi}{2} \right) \right], \quad \hat{t} = (p_a - p_c)^2, \quad (6)$$

where θ_π is the angle from the beam direction in the laboratory frame. The bounds of the integral over η , η_{\max} and η_{\min} , are given by the experimental condition. Using Madelstam variables $s = (p_A + p_B)^2$, $t = (p_A - p_\pi)^2$, and $u = (p_B - p_\pi)^2$, we define variables x_1 and x_2 [17]:

$$x_1 \equiv -\frac{u}{s} = \frac{x_T}{2} e^{+\eta}, \quad x_2 \equiv -\frac{t}{s} = \frac{x_T}{2} e^{-\eta}, \quad (7)$$

where x_T is given by $x_T = 2p_T/\sqrt{s}$. The lower bounds of the integrals and the variable z_c are then expressed:

$$x_a^{\min} = \frac{x_1}{1 - x_2}, \quad x_b^{\min} = \frac{x_a x_2}{x_a - x_1}, \quad z_c = \frac{x_1}{x_a} + \frac{x_2}{x_b}. \quad (8)$$

The polarized cross section in Eq. (5) is calculated by these expressions together with polarized PDFs and fragmentation functions. The unpolarized cross section $d\sigma/dp_T$ is calculated in the similar way. In calculating the NLO cross sections, K -factors are simply multiplied in order to obtain them from the leading-order (LO) ones as was done in unpolarized PDF analyses [18]. We employed $K=1.0$ and 1.6 for the polarized and unpolarized cross sections, respectively, basing on more detailed analyses in Ref. [15]. This approximation inevitably introduces systematic uncertainties from the p_T dependence of the K factor and the choice of the PDF set. Such an error is estimated to be $\sim 20\%$ in the cross sections, which is comparable magnitude to a typical scale uncertainty in this energy region. A possible criticism to K -factor approach in PDF analysis might be a change in corresponding x -region due to higher-order corrections, which should be the origin of the K -factor. Since the cross section drops rapidly with increasing p_T , which is a good measure of relevant x region especially for the PHENIX acceptance covering only central rapidity, changes in the cross section would correspond to small change in p_T even

if the change is fully attributed to a shift in p_T . For example, 50% changes in the cross section can be obtained by 10% change in p_T . Therefore, we think the uncertainty involved in the x -determination due to K -factor approach is smaller compared to other uncertainties. Clearly more precise procedure has to be applied as the precision of experimental data improves.

The polarized PDFs are expressed by a number of parameters and unpolarized PDFs at a fixed Q^2 ($\equiv Q_0^2$):

$$\Delta f(x, Q_0^2) = [\delta x^\nu - \kappa(x^\nu - x^\mu)]f(x, Q_0^2), \quad (9)$$

where δ , κ , ν , and μ are parameters to be determined by a χ^2 analysis, and $f(x)$ is the corresponding unpolarized PDF. Assuming flavor-symmetric polarized antiquark distributions $\Delta \bar{u} = \Delta \bar{d} = \Delta \bar{s} \equiv \Delta \bar{q}$ at Q_0^2 , we determine four polarized distributions, Δu_v , Δd_v , $\Delta \bar{q}$, and Δg , which are expressed by the parameters in Eq. (9). As usual in this kind of analysis, the first moments of Δu_v and Δd_v are fixed by semileptonic decay data of octet baryons: $\int dx \Delta u_v = 0.926$, $\int dx \Delta d_v = -0.341$ [1, 2].

The positivity condition $|\Delta f(x)| \leq f(x)$ is imposed in the initial PDFs. It should be satisfied in the LO, whereas it does not have to be strictly satisfied in the NLO due to NLO corrections. The details of the NLO corrections on the positivity condition are discussed in Ref. [19]. We have imposed the condition only for a practical reason to avoid unphysical solutions particularly at large x . When the precision of experimental data is improved, we should be able to release this condition. A recent unpolarized gluon distribution [18, 20] becomes negative at small x (< 0.01) and Q^2 (~ 1 GeV²), a special attention should be paid to the condition. In such a region, few polarized data are used in our analysis at this stage, so that the positivity condition does not affect the analysis significantly.

The parameters of the polarized PDFs are determined so as to minimize the total χ^2 :

$$\chi^2 = \sum_i \frac{[A_i^{\text{data}}(x, Q^2) - A_i^{\text{calc}}(x, Q^2)]^2}{[\Delta A_i^{\text{data}}(x, Q^2)]^2}, \quad (10)$$

where A_i^{data} indicates the spin-asymmetry data for A_1 and $A_{LL}^{\pi^0}$; A_i^{calc} is the theoretically calculated asymmetry at the same Q^2 point. The polarized and unpolarized PDFs at Q_0^2 are evolved to the experimental Q^2 point by the standard DGLAP (Dokshitzer-Gribov-Lipatov-Altarelli-Parisi) evolution equations [21]. The experimental error ΔA_i^{data} is given by systematic and statistical errors: $(\Delta A_i^{\text{data}})^2 = (\Delta A_i^{\text{stat}})^2 + (\Delta A_i^{\text{systr}})^2$. The total χ^2 is minimized by the CERN program library MINUIT [22].

The uncertainties of the polarized PDFs are estimated by the Hessian method [23]. We express the parameters as a_i ($i=1, 2, \dots, N$), where N is the number of the parameters, and the minimum point of χ^2 is denoted \hat{a} . Then, the uncertainty of a distribution $F(x)$ is calculated

by

$$[\delta F(x)]^2 = \Delta \chi^2 \sum_{i,j} \left(\frac{\partial F(x, \hat{a})}{\partial a_i} \right) H_{ij}^{-1} \left(\frac{\partial F(x, \hat{a})}{\partial a_j} \right), \quad (11)$$

where H_{ij} is the Hessian. The value of $\Delta \chi^2$ is given by $\Delta \chi^2 = 12.65$ so that the uncertainty indicates the one- σ -error range for eleven free parameters [2]. The details of this $\Delta \chi^2$ choice are discussed in a number of publications [24].

III. RESULTS

We determine the parameters by minimizing the total χ^2 in Eq. (10). In order to find an impact of the RHIC- $A_{LL}^{\pi^0}$ data on the polarized PDF determination, we tried two types of analyses:

- Type 1: with the DIS- A_1 and RHIC- $A_{LL}^{\pi^0}$ data,
- Type 2: with only the DIS- A_1 data.

For the theoretical π^0 production calculations, the kinematical conditions, $\sqrt{s}=200$ GeV and $|\eta| \leq 0.35$, are used. The initial Q^2 point is taken as $Q_0^2 = 1$ GeV². We have tried another fit with $Q_0^2 = 0.8$ GeV², but there was no difference in the results. The number of flavor is three. The longitudinal-transverse ratio R in Eq. (1) is taken from the SLAC parametrization [25]. The GRV98 parametrization [26] is used for the unpolarized PDFs. We also tested other distributions; however, the obtained polarized PDFs did not change conspicuously. It is because the differences in the PDFs could be absorbed into the parametrized function in Eq. (9) by minor adjustments of the parameters.

The obtained parameters are tabulated in Table I. [45] Their values are similar to those of the previous version [2]. The small- x behavior of the polarized antiquark distributions cannot be determined by the current experimental data, so that the parameter $\mu_{\bar{q}}$, which determined the small- x behavior, is fixed at $\mu_{\bar{q}} = 1$ as in Ref. [2]. Because the first moments of Δu_v and Δd_v are fixed, there are no errors in the parameters κ_{u_v} and κ_{d_v} .

The χ^2 values for the used data set are listed in Table II. The data set includes the measurements from EMC (European Muon Collaboration) [27], SMC [28], SLAC-E130, E143, E154, E155 [29], HERMES [11, 30], JLab Hall-A, [10], COMPASS [12], and PHENIX [8] collaborations. The additional data, which were not used in the AAC03 analysis, are the ones from JLab [10], HERMES [11], COMPASS [12], and PHENIX [8]. In two different analyses, similar $\chi^2/\text{d.o.f.}$ values are obtained. As we will see later, two fit results show almost the same $\Delta u_v(x)$, and slight changes in the central curves of $\Delta d_v(x)$, $\Delta \bar{q}(x)$, and $\Delta g(x)$. The major difference is in the uncertainty bands for antiquark and gluon distributions.

TABLE I: Obtained parameters by the χ^2 analyses.

distribution	δ	ν	κ	μ
Type 1: DIS and π^0 data				
Δu_v	0.959 ± 0.099	0.0 (fixed)	0.588	1.048 ± 0.266
Δd_v	-0.773 ± 0.210	0.0 (fixed)	-0.478	1.243 ± 0.561
$\Delta \bar{q}$	0.780 ± 0.904	1.014 ± 0.180	-75.9 ± 11.2	1.0 (fixed)
Δg	-1.00 ± 4.39	2.74 ± 1.30	252 ± 139	2.70 ± 2.57
Type 2: DIS data only				
Δu_v	0.958 ± 0.101	0.0 (fixed)	0.585	1.056 ± 0.272
Δd_v	-0.768 ± 0.204	0.0 (fixed)	-0.474	1.218 ± 0.552
$\Delta \bar{q}$	0.955 ± 0.951	1.014 ± 0.185	-82.7 ± 13.2	1.0 (fixed)
Δg	-1.00 ± 3.28	2.30 ± 0.883	253 ± 153	2.27 ± 1.75

 TABLE II: Numbers of the A_1 data and χ^2 values are listed for the two types of analyses. The notations p , n , and d indicate proton, neutron, and deuteron, respectively.

data set	x range	Q^2 range (GeV ²)	No. of data	χ^2	
				Type 1 DIS- A_1 + $A_{LL}^{\pi^0}$	Type 2 DIS- A_1 only
EMC (p)	0.015–0.466	3.50–29.5	10	4.84	4.81
SMC (p)	0.004–0.484	1.14–72.10	59	55.72	55.21
E130 (p)	0.19–0.64	5.32–9.91	8	4.74	4.72
E143 (p)	0.027–0.749	1.17–9.52	81	61.56	60.78
E155 (p)	0.015–0.750	1.22–34.72	24	32.41	32.88
HERMES (p)	0.033–0.447	1.22–9.18	9	3.32	3.31
SMC (d)	0.0042–0.483	1.14–71.76	65	57.68	57.16
E143 (d)	0.027–0.749	1.17–9.52	81	88.33	89.13
E155 (d)	0.015–0.750	1.22–34.79	24	18.22	18.26
HERMES (d)	0.033–0.446	1.22–9.16	9	12.62	11.88
COMPASS (d)	0.051–0.474	1.18–47.5	12	9.18	8.99
E142 (n)	0.035–0.466	1.1–5.5	8	2.90	2.76
E154 (n)	0.017–0.564	1.21–15.0	11	3.13	3.36
HERMES (n)	0.033–0.464	1.22–5.25	9	2.14	2.18
J-Lab (n)	0.33–0.60	2.71–4.83	3	2.50	2.63
DIS total			413	359.29	358.05
PHENIX (π^0)			8	11.18	–
total χ^2 (χ^2 /d.o.f.)			421	370.47 (0.904)	358.05 (0.891)

A. Comparison with spin asymmetry measurements

We compare the resulted parametrization with newly added experimental data of DIS and π^0 production in pp collisions. Since the agreement with other data is found to be maintained, we do not show here.

First, the parametrization results of the type-1 are compared with inclusive DIS data by JLab, HERMES, and COMPASS on the spin asymmetry A_1 in Fig. 1, where actual differences between the theoretical asymmetries and experimental data ($A_1^{\text{data}} - A_1^{\text{theo}}$) are shown. The theoretical asymmetry A_1^{theo} is calculated at the experimental Q^2 point of A_1^{data} . The AAC03 uncertainty bands are shown by the solid curves and the current AAC06 type-1 uncertainty ranges are by the shaded areas. The uncertainties are calculated at $Q^2=5$ GeV². It is obvious from this figure that the HERMES and COMPASS data on

A_1^p and A_1^d significantly reduced (about 50%) the uncertainties of the asymmetries in the region, $x \sim 0.2$. On the other hand, the JLab data play an important role in reducing the uncertainty for the neutron in the region, $x \gtrsim 0.2$. These data are valuable for a better determination of the polarized quark and antiquark distributions as shown in Sec. III B.

Second, the analysis results are compared with the PHENIX data on the pion-production asymmetry $A_{LL}^{\pi^0}$ [8] in Fig. 2. The theoretical curves and their uncertainties are shown for the type 1 and 2 analyses. The hard scale is taken as $Q^2 = p_T^2$ in calculating the PDF and their uncertainties, and the KKP (Kniel, Kramer, and Pötter) fragmentation functions [31] are used. It is known from more detailed analysis that the choice does not change the asymmetries [32]. It is clear from Fig. 2 that the PHENIX data should significantly improve the uncertainties in the PDFs, mainly the polarized gluon distribution

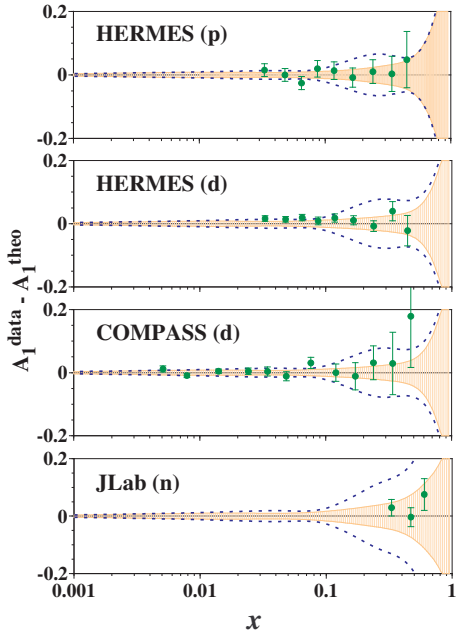


FIG. 1: (Color online) Differences between the data and parametrization results. The dotted curves indicate uncertainty bands of the AAC03 analysis and the shaded areas are the bands of the current analysis.

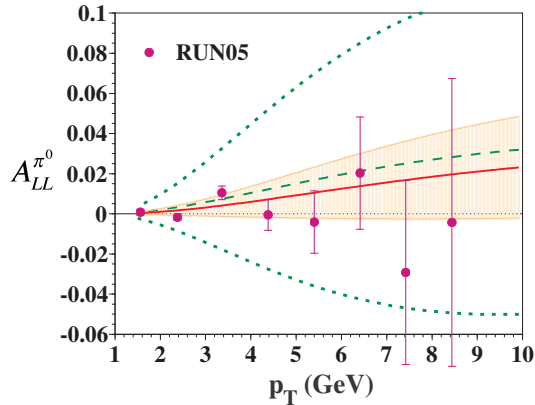


FIG. 2: (Color online) Comparison with PHENIX π^0 -production asymmetry data $A_{LL}^{\pi^0}$. The solid and dashed curves indicate type 1 and 2 analysis results, respectively. The uncertainty range for the type 1 is shown by the shaded band, and the one for the type 2 is by the dotted curves.

as we will see later. However, the resulted PDFs are still consistent with $A_{LL}^{\pi^0} = 0$ in the entire p_T region, and it suggests a need of more precise data. Nevertheless, significantly improved constraints on the gluon distribution will be discussed basing on this fit results in Sec. III B.

In order to illustrate the current precision of the structure function g_1 for the proton, the experimental data are compared with the fit results including uncertainty bands in Fig. 3. Here, only the type-1 results are shown. Experimental measurements are usually listed

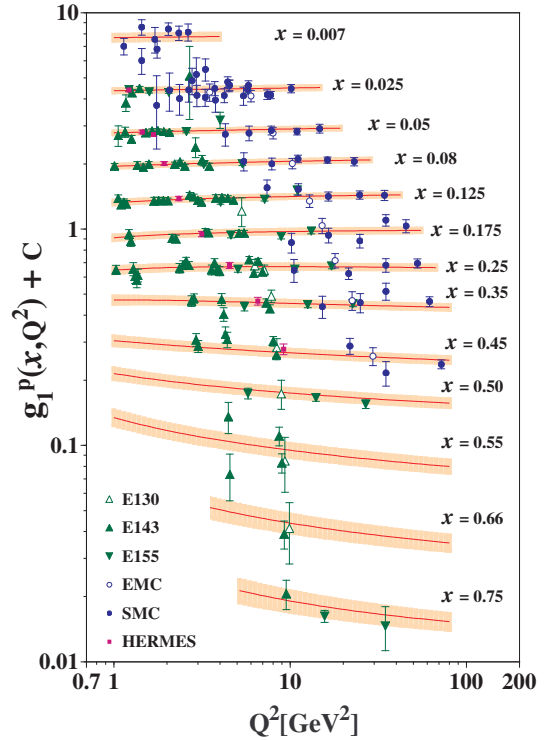


FIG. 3: (Color online) Current type-1 analysis results are compared with g_1^p data.

by the spin asymmetry A_1 , so that the g_1^p data are calculated by using the unpolarized PDFs of the GRV98 [26] and the SLAC parametrization for R with Eq. (1). We notice that the uncertainty bands are still wide at large x (>0.5). The smaller x region ($x < 0.007$) still remains unmeasured. Although the kinematical coverage of the experimental data are being extended, precision data are missing especially in the large- x and extremely small- x regions, especially when we compared with the HERA data [33]. Wider kinematical coverage is essential in extraction of Δg through a scaling violation. Such measurement would be feasible at the proposed polarized ep -colliders, e-LIC [34] or eRHIC [35].

B. Polarized parton distribution functions

The polarized PDFs obtained by the analyses are shown in Fig. 4 at $Q^2=1$ GeV², and they are compared with the AAC03 distributions. Their uncertainties are also shown. The distributions are almost the same in both analyses; however, there are much differences between the uncertainty bands. Although the Δu_v uncertainty bands are the same, the Δd_v determination is improved at $x > 0.2$ due to the JLab neutron data. The polarized antiquark distribution is significantly improved at $x \sim 0.1$ because of HERMES and COMPASS data on the deuteron.

The most significant improvement is found for the po-

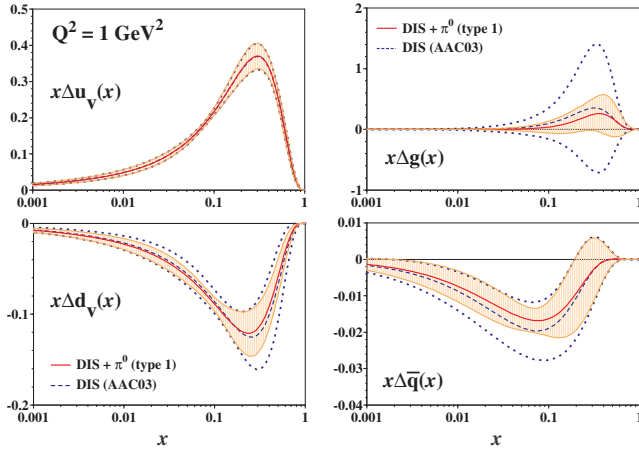


FIG. 4: (Color online) Polarized PDFs obtained by the type-1 χ^2 analysis are shown at $Q^2=1$ GeV² by the solid curves, and their uncertainties are shown by the shaded bands. In comparison, the AAC03 PDFs are shown by the dashed curves and their uncertainties by the dotted curves.

larized gluon distribution. As clearly shown Fig. 4, the uncertainties in gluon polarization are significantly reduced in the type-1 fit, where the A_{LL} for pion production is included. The central curve also shifted slightly. The AAC03 analysis indicated that a negative gluon polarization is possible; however, we clearly see some preference for the positively polarized gluon in the type-1 analysis. We have found a possibility that $\Delta g(x)$ at large x could be constrained by the g_1^d data from the HERMES and COMPASS collaborations. The impact of newly obtained data will be further discussed in Sec. IV.

The first moments of $\Delta\bar{q}(x)$, $\Delta g(x)$, and $\Delta\Sigma(x) = \sum_i [q_i(x) + \bar{q}_i(x)]$ are listed at $Q^2=1$ GeV² in Table III together with the ones of the AAC03. Because the quark and antiquark distributions are almost the same as the AAC03, the first moment of $\Delta\bar{q}$ and the quark spin content $\Delta\Sigma$ are similar in the current and AAC03 analyses. The only difference is the gluon first moment. First, the uncertainty of Δg is significantly reduced in the type-1 analysis ($1.27 \rightarrow 0.32$). This is because of the PHENIX data, which constrain the polarized gluon distribution in the region $x \sim 0.1$. Therefore, the PHENIX $A_{LL}^{\pi^0}$ measurements play an important role in the determination of $\Delta g(x)$. However, it should be mentioned that an effect from the assumed functional form is not included in estimating the uncertainty. Furthermore, there is an additional scale uncertainty due to the scale error of the PHENIX data (40%) originated predominantly in the beam polarization uncertainty. This uncertainty is estimated to be $\sim 20\%$ in $\Delta g(x)$ and its first moment, while the quark sector remains intact.

The polarized PDFs are compared with other recent distributions at $Q^2=1$ GeV² in Fig. 5. The solid, dashed, dashed-dot, dotted curves indicate AAC06 (type-1 analysis), GRSV (Glück, Reya, Stratmann, and Vogelsang) [36], BB (Blümlein and Böttcher) [37], and LSS (Leader,

TABLE III: The first moments of the obtained polarized PDFs at $Q^2 = 1$ GeV². The current analysis results are compared with those of the previous results (AAC03). The $\Delta\Sigma$ is the quark spin content.

	$\Delta\bar{q}$	Δg	$\Delta\Sigma$
Type 1	-0.05 ± 0.01	0.31 ± 0.32	0.27 ± 0.07
Type 2	-0.06 ± 0.02	0.47 ± 1.08	0.25 ± 0.10
AAC03	-0.06 ± 0.02	0.50 ± 1.27	0.21 ± 0.14

Sidorov, and Stamenov) [38] distributions, respectively. All the distributions agree well except for the polarized gluon distribution. However, the uncertainty band of $\Delta g(x)$ is still huge even if the PHENIX-pion data are included in the analysis. The different distributions agree each other because they are roughly within the uncertainties. The various parametrizations have different analysis methods such as in the used data set, x -dependent functional form, treatment of higher-twist effects, and positivity condition; however, the obtained distributions are similar. There are other recent parametrization studies [39] with semi-inclusive data by de Florian, Navarro, and Sassot and also in the statistical-parton-distribution model by Bourrely, Soffer, and Buccella although they are not shown in the figure. There are also other parametrization studies in Ref. [40].

Next, the polarized antiquark distribution of the type-1 is compared with experimental antiquark-distribution ratios $\Delta\bar{u}/\bar{u}$, $\Delta\bar{d}/\bar{d}$, and $\Delta\bar{s}/\bar{s}$ by the HERMES collaboration [41] in Fig. 6. The HERMES measured semi-inclusive spin asymmetries for pion and kaon productions in positron and electron DIS with proton and deuteron targets. They analyzed the semi-inclusive data together with the inclusive ones on A_1 for obtaining the quark and antiquark distribution ratios, $\Delta q(x)/q(x)$ and $\Delta\bar{q}(x)/\bar{q}(x)$, in the LO. Effects of NLO radiative corrections are small

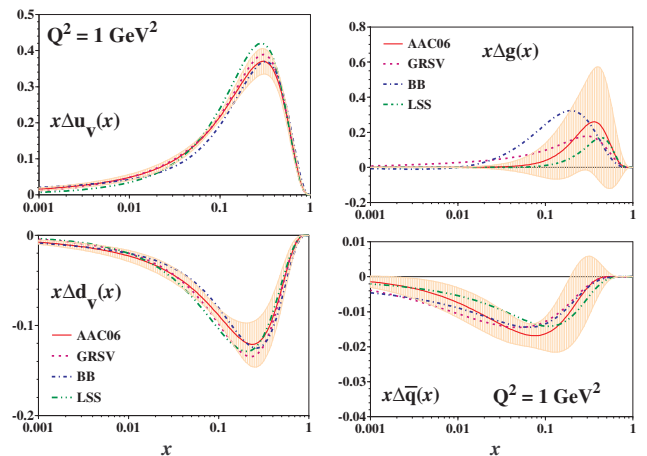


FIG. 5: (Color online) Comparison with other polarized PDFs at $Q^2=1$ GeV². The type 1 distributions and their uncertainties are shown by the solid curves and bands. The others are the GRSV, BB, and LSS parametrizations.

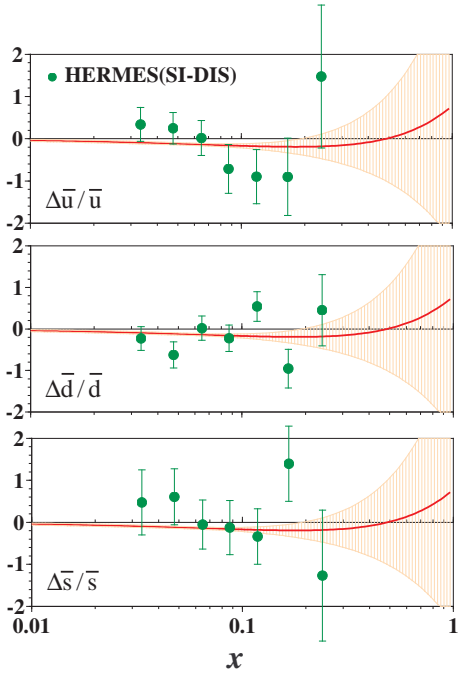


FIG. 6: (Color online) Comparison with the HERMES semi-inclusive DIS data on the antiquark distribution ratios $\Delta\bar{u}/\bar{u}$, $\Delta\bar{d}/\bar{d}$, and $\Delta\bar{s}/\bar{s}$. The solid curves are the type-1 analysis results at $Q^2=1$ GeV² and the uncertainty ranges are shown by the shaded bands.

in comparison with the experimental errors because the distribution ratios are taken. Therefore, although the experimental ratios are obtained by LO analyses and the theoretical ratios are calculated in the NLO, they can be compared with each other. In the AAC analyses, flavor symmetric antiquark distributions are assumed $\Delta\bar{u}(x) = \Delta\bar{d}(x) = \Delta\bar{s}(x)$ at $Q^2=1$ GeV²; however, one should note that the antiquark distributions are different ($\Delta\bar{u}(x) \neq \Delta\bar{d}(x) \neq \Delta\bar{s}(x)$) at $Q^2 \neq 1$ GeV² because of Q^2 evolution effects in the NLO [42]. In the figure, the type-1 distributions are shown at $Q^2=1$ GeV²; however, Q^2 variations are small because the ratios are taken. The theoretical antiquark-distribution ratios agree with the HERMES data if the experimental errors and the parametrization uncertainties are considered. At this stage, the semi-inclusive data are not included in the global analysis. The data are fully consistent with our parametrization. It is obvious that the data would impose significant constraints when the data precision is improved.

The AAC00 and AAC03 codes are available at the web site [2] for calculating the polarized PDFs. However, such a library is not prepared for the current analyses because the PHENIX data utilized here are still preliminary results. In particular, the data will become more accurate in the final paper, so that the $\Delta g(x)$ uncertainty should become smaller. After the data are finalized, we plan to provide a code for the polarized PDFs.

IV. POLARIZED GLUON DISTRIBUTION

In this section, the details are discussed on the determination of the polarized gluon distribution. First, we explain the possibility that the recent HERMES and COMPASS measurements on A_1^d could impose a constraint for $\Delta g(x)$ at large x because of their Q^2 differences. Second, the possibility of negative gluon distribution ($\Delta g(x) < 0$) at small x is studied by including the PHENIX π^0 data in the analysis. Third, the polarized gluon distributions obtained by the current analyses are compared with HERMES, SMC, and COMPASS measurements on the ratio $\Delta g(x)/g(x)$.

A. Polarized gluon distribution at large x

We discuss the possibility that precise measurements of g_1 at $x \sim 0.05$ could impose a constraint on $\Delta g(x)$ at larger x . As shown in Eq. (2), the structure function is given by the convolution integral of the polarized PDFs with corresponding coefficient functions. In particular, we discuss an effect of the gluon term $(x/z)\Delta g(x/z)\Delta C_g(z)$, where z is the integration variable in Eq. (3).

The parametrization results of the type 1 are compared with inclusive DIS data particularly by JLab, HERMES, and COMPASS on the spin asymmetry A_1 . Then, the parametrization is consistent with the SLAC-E154 neutron data and COMPASS deuteron data. Although the agreement is excellent also with the HERMES proton data for A_1^p , the curve deviates at small x ($0.03 < x < 0.07$) in the HERMES deuteron data (A_1^d).

It is noteworthy that the central curve of our fit results deviates from HERMES A_1^d at small x , although a reasonable agreement is obtained with COMPASS A_1^d in the same x -region. The deviation from the HERMES data points becomes larger when we artificially remove

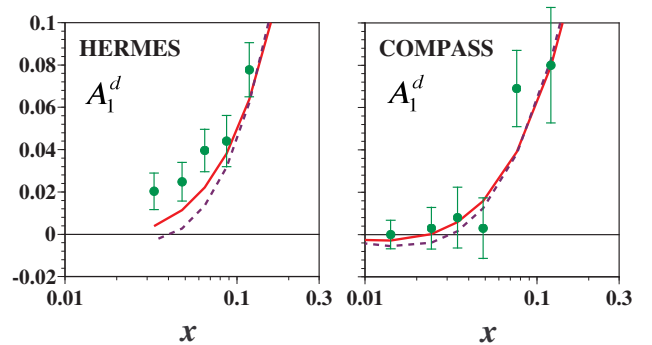


FIG. 7: (Color online) The HERMES and COMPASS data on the spin asymmetry of the deuteron (A_1^d) at small x are shown in comparison with the parametrization results. The solid curves indicate the type-1 asymmetries and the dashed ones are obtained simply by removing the NLO gluon term ($\Delta C_g = 0$) in the structure function g_1 .

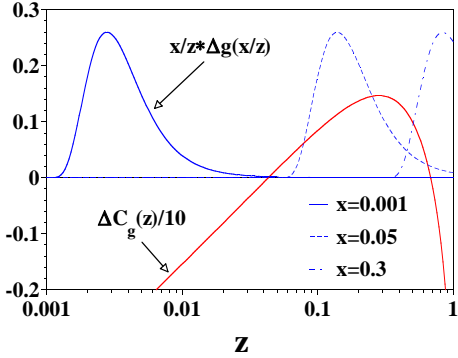


FIG. 8: (Color online) The polarized gluon distributions and coefficient function are shown at $x=0.001$, 0.05 , and 0.3 for the type-1 parametrization.

the gluon contribution to g_1^d , which is shown as dashed curves in Fig. 7. Because the Q^2 values are quite different: $Q_{\text{HERMES}}^2 = 1 \text{ GeV}^2$ and $Q_{\text{COMPASS}}^2 = 6 \text{ GeV}^2$, we could attribute the observed discrepancy to the Q^2 difference. There are two possible effects of such kind; one is the higher-twist effect as pointed out recently in Ref. [38]. The other, which we found in this analysis, is due to a *positive gluon polarization at large x* , which we discuss below.

We recall the gluon contribution to the g_1 is $(x/z)\Delta g(x/z)\Delta C_g(z)$ integrated with respect to z over $(x, 1)$. In this picture, the gluon with the momentum fraction x/z would split into the quark with a momentum fraction x and anything else to contribute to the $g_1(x)$. Figure 8 displays the type-1 polarized gluon distribution $(x/z)\Delta g(x/z)$ for selected x -values and the polarized coefficient function $\Delta C_g(z)$ as functions of z . The $\Delta C_g(z)$ is positive in the region, $0.05 < z < 0.7$, whereas it is negative in other z region. The function $(x/z)\Delta g(x/z)$ for $x = 0.001$ peaks at around $z = 0.002$ and it moves to a larger z as x becomes larger ($x=0.05$ and 0.3). Therefore, the gluon contribution to the g_1 is negative in the small- x region, positive at medium x (~ 0.05), and back to negative at large x .

The HERMES data shows a discrepancy from our parametrization result with the gluon contribution eliminated especially in the region, $0.033 \leq x \leq 0.065$. This is the x region where the gluonic contribution from $\Delta g(x) > 0$ is positive. If the Δg is negative, the gluonic contribution to g_1 will be negative so that the discrepancy becomes larger. Therefore, we could interpret the deviation of HERMES data as an indication of positive $\Delta g(x)$ at large x .

Obviously further precision studies are necessary to identify the source of the discrepancy. Determination of the sign of the gluon polarization will be helpful. More precise data on the Q^2 dependence of g_1 would be certainly helpful, too.

B. Polarized gluon distribution at small x

We have discussed the polarized gluon distribution at large x basing on Q^2 dependence of A_1^d . On the other hand, the gluon polarization in small- x region is not obvious. Most of the global analyses showed $\Delta g(x) > 0$ in the small- x region, and estimated uncertainty turned out to be small including our previous analysis, BB, and LSS. We are going to show that different small- x behavior is still allowed within the current framework, and that the uncertainty band changes drastically.

We start from the possibility of negative gluon polarization inspired from the two possible solutions of $\Delta g(x)/g(x)$ to reproduce $A_{LL}^{\pi^0}$ measured by PHENIX. Since the pion production is dominated by gg scattering at small p_T , the asymmetry $A_{LL}^{\pi^0}$ approximately depends on quadratic function of $\Delta g(x)/g(x)$. Indeed, two solutions, positive and negative $\Delta g(x)/g(x)$ can be obtained, when only $A_{LL}^{\pi^0}$ data are used to constrain $\Delta g(x)/g(x)$

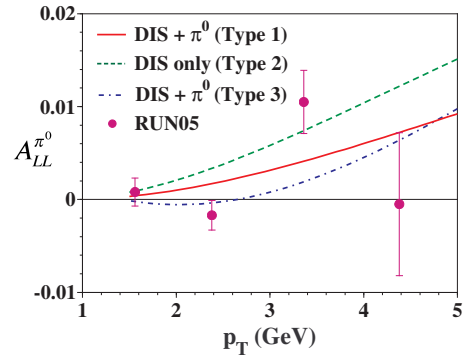


FIG. 9: (Color online) Theoretical asymmetries are shown for the type 1, 2, and 3 parametrizations in comparison with the PHENIX data of $A_{LL}^{\pi^0}$. Only the small- p_T region is shown in order to see the differences between the theoretical asymmetries at small p_T .

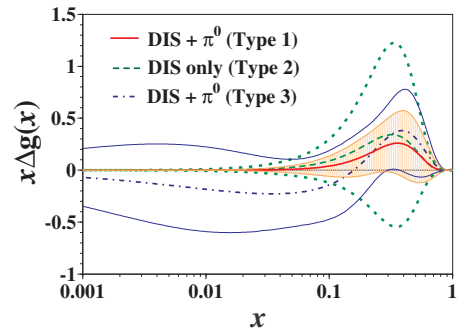


FIG. 10: (Color online) The polarized gluon distributions are shown at $Q^2=1 \text{ GeV}^2$. The solid, dashed, and dotted curves indicate the type 1, 2, and 3 distributions, respectively. The uncertainty ranges are shown by the shaded band, the dotted curves, and the thin solid curves for the type 1, 2 and 3, respectively.

[15, 43]. The PHENIX $A_{LL}^{\pi^0}$ is sensitive to the gluon around $x \sim 0.1$, and the negative $\Delta g(x)/g(x)$ solution can coexist with the previously mentioned positive $\Delta g(x)$ at large x .

To explore this possibility, we have performed another global fit by assigning the initial distribution, $\Delta g(x) = -\Delta g(x)_{\text{type-1}}$, at Q_0^2 without modifying the parametrization in Eq. (9). The fit was successful, and there was no practical difference in χ^2 . The resulted parameter set is referred to as type 3. The fit results are shown in Fig. 9 in comparison with the type-1 and 2 parametrizations and the PHENIX experimental data on the double spin asymmetry $A_{LL}^{\pi^0}$. For explaining the negative asymmetry at $p_T=2.38$ GeV, a significant change of the functional form of $\Delta g(x)$ is needed in the region, $0.06 < x < 0.2$. There is no noticeable change in the quark distributions and only $x\Delta g(x)$ is shown in Fig. 10. As can be expected from the discussion above, the $\Delta g(x)$ is negative up to $x \sim 0.1$ and retains positive value towards larger x region especially to reproduce Q^2 dependence of A_1^d .

Three types of the gluon polarization $\Delta g(x)$ are displayed with their uncertainties in Fig. 10. The uncertainty bands are reduced in the analyses with the pion data. In principle, $\Delta g(x)$ should be constrained only in the PHENIX kinematical range $x \sim 0.1$. However, the reduction is also found in the region $x > 0.2$. This is because a smooth functional form is assumed in the analysis, where the constraint in the $x \sim 0.1$ region also affects the uncertainty estimation in other x regions. Because the gluon-gluon subprocesses dominate, the polarized cross section for pion-production depends on Δg quadratically. It leads to two independent solutions, the type 1 and type 3. In the region $x \gtrsim 0.1$ partially covered by the PHENIX data, similar uncertainties are obtained and they cover both solutions. However, the type-3 $\Delta g(x)$ resides outside of the uncertainty bands of type 1 and type 2 at small x , which reveals that the uncertainty depends on the functional behavior of $\Delta g(x)$. The errors due to this functional form are not included in showing the uncertainty bands in our analysis and also other ones [37, 38], because there is no systematic way to include them.

The large uncertainty in type-3 $\Delta g(x)$ in the smaller- x region is also reflected to the first moment: -0.56 ± 2.16 . The large error comes from the small- x region, where there is no experimental data which constrains the small- x behavior of $\Delta g(x)$. In fact, if the type-3 $\Delta g(x)$ is integrated over the region, $0.1 \leq x \leq 1$, covered by the DIS and pion-production data, the first moment becomes 0.32 ± 0.42 which is comparable to the type-1 value, 0.30 ± 0.30 , in the same x region. Only the Q^2 evolution and smoothness of functional forms are the possibilities to provide some constraints in the small- x region. Please note that there is no direct experimental constraint for $\Delta g(x)$ at small x , therefore it is highly unconstrained. In order to clarify the situation, we need a definitive measurement of the sign of the gluon polarization around $x \lesssim 0.1$. The higher energy run ($\sqrt{s} = 500$ GeV) at

RHIC and eRHIC/e-LIC would play important roles in such measurements.

C. Comparison with high- p_T hadron-production data in DIS

There are reports on the polarized gluon distribution from high- p_T hadron production in DIS by HERMES [3], SMC [4], and COMPASS [5] collaborations. Their data are shown by the ratio $\Delta g(x)/g(x)$. There are also preliminary data by the COMPASS [6] for $\Delta g(x)/g(x)$ from analyses of high- Q^2 (>1 GeV²) hadron-production and charmed-hadron-production data.

We compare our results with those experimental data in Fig. 11. The parametrization results for the type 1, 2, and 3 are shown together with their uncertainty bands. The high- p_T hadron data in DIS impose a constraint for the polarized gluon distribution in the x range, $0.07 < x < 0.2$. We find that three fit results are consistent with these data within both uncertainties.

It is interesting to note that the $\Delta g(x)/g(x)$ distributions obtained by the analyses are similar to a theoretical prediction by Brodsky and Schmidt [44] in the region, $x \sim 0.1$.

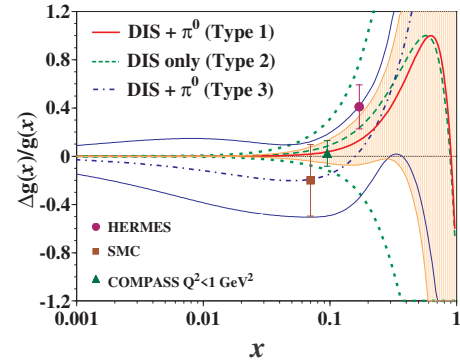


FIG. 11: (Color online) The theoretical ratios $\Delta g(x)/g(x)$ of the type 1, 2, and 3 are compared with high- p_T hadron-production data measured in DIS by HERMES, SMC, and COMPASS collaborations. The solid, dashed, and dashed-dot curves indicate type 1, 2, and 3 parametrization results, respectively. The uncertainty ranges are shown by the shaded band, the dotted curves, and the thin solid curves for the type 1, 2 and 3, respectively.

V. SUMMARY

We have performed the global analysis of spin asymmetry data from DIS and neutral-pion production in polarized pp scattering. First, we showed two types of analysis results by using DIS and PHENIX pion data and by using only the DIS data. In comparison with the previous version (AAC03), new data are added from the JLab A_1^n ,

HERMES and COMPASS A_1^d , and PHENIX $A_{LL}^{\pi^0}$ measurements. We found that the JLab neutron data contribute to reduce the uncertainty band of the valence distribution Δd_v , the HERMES and COMPASS data to improve the antiquark distribution $\Delta \bar{q}$ in the region, $x \sim 0.1$.

There are two important consequences on the polarized gluon distribution. First, the differences between the HERMES and COMPASS A_1^d data could indicate a positive gluon polarization at large x because of their Q^2 differences. Second, the PHENIX $A_{LL}^{\pi^0}$ measurements improve the determination of $\Delta g(x)$ significantly. In fact, the uncertainty band of $\Delta g(x)$ becomes smaller by 60%.

Acknowledgments

This work is supported by the Grant-in-Aid for Scientific Research from the Japanese Ministry of Education, Culture, Sports, Science, and Technology. It is also supported by RIKEN and the Japan-U.S. Cooperative Science Program. The authors thank K. Sudoh and the entire RHIC Spin Collaboration, especially A. Bazilevsky, A. Deshpande, Y. Fukao, M. Stratmann, and W. Vogelsang, for helpful discussions on the gluon polarization.

-
- [1] Asymmetry Analysis Collaboration (AAC), Y. Goto, N. Hayashi, M. Hirai, H. Horikawa, S. Kumano, M. Miyama, T. Morii, N. Saito, T.-A. Shibata, E. Taniguchi, T. Yamaniishi, Phys. Rev. **D62**, 034017 (2000).
- [2] Asymmetry Analysis Collaboration (AAC), M. Hirai, S. Kumano, N. Saito (AAC), Phys. Rev. **D69**, 054021 (2004). The AAC code for polarized PDFs is available at <http://spin.riken.bnl.gov/aac/>.
- [3] HERMES collaboration, A. Airapetian *et al.*, Phys. Rev. Lett. **84**, 2584 (2000).
- [4] Spin Muon Collaboration (SMC), B. Adeva *et al.*, Phys. Rev. **D70**, 012002 (2004).
- [5] COMPASS collaboration, E. S. Ageev *et al.*, hep-ex/0511028.
- [6] F. Bradamante, talk given at the workshop on Hadron Structure at J-PARC, Nov. 30 - Dec. 2, 2005, KEK, Tsukuba, Japan, <http://www-conf.kek.jp/J-PARC-HS05/>.
- [7] PHENIX collaboration, S. S. Adler *et al.*, Phys. Rev. Lett. **93**, 202002 (2004).
- [8] PHENIX collaboration, K. Boyle, talk at the XVIIth Particles and Nuclei International Conference (PANIC05), <http://www.panic05.lanl.gov/>.
- [9] STAR collaboration, J. Koryluk, hep-ex/0512040.
- [10] Jefferson Lab Hall A collaboration, X. Zheng *et al.*, Phys. Rev. Lett. **92**, 012004 (2004)
- [11] HERMES collaboration, A. Airapetian *et al.*, Phys. Rev. **D71**, 012003 (2005).
- [12] COMPASS collaboration, E. S. Ageev *et al.*, Phys. Lett. **B612**, 154 (2005).
- [13] R. Devenish and A. Cooper-Sarkar, *Deep Inelastic Scattering*, Oxford University press (2004). See also, for example, Ref. [27].
- [14] Expressions of NLO corrections are found, for example, in M. Hirai, S. Kumano, and M. Miyama, Comput. Phys. Commun. **108**, 38 (1998).
- [15] B. Jäger, A. Schäfer, M. Stratmann, and W. Vogelsang, Phys. Rev. **D67**, 054005 (2003); B. Jäger, M. Stratmann, S. Kretzer, and W. Vogelsang, Phys. Rev. Lett. **92**, 121803 (2004); M. Hirai and K. Sudoh, Phys. Rev. **D71**, 014022 (2005).
- [16] E. Leader, *Spin in Particle Physics*, Cambridge University Press (2001).
- [17] R. D. Field, *Applications of perturbative QCD*, Addison-Wesley Publishing Company (1989).
- [18] J. Pumplin, D. R. Stump, J. Huston, H. L. Lai, P. Nadolsky, and W. K. Tung, JHEP, **0207**, 012 (2002); See T. Kluge, K. Rabbertz, and M. Wobisch, talk at the TeV4LHC workshop, CERN, Switzerland, April 28-30, 2005.
- [19] G. Altarelli, S. Forte, and G. Ridolfi, Nucl. Phys. **B534**, 277 (1998).
- [20] A. D. Martin, R. G. Roberts, W. J. Stirling, and R.S. Thorne, Phys. Lett. **B604**, 61 (2004); S. Alekhin, JETP Lett. **82**, 628 (2005).
- [21] Q^2 evolution programs are discussed in Ref. [14] and M. Miyama and S. Kumano, Comput. Phys. Commun. **94**, 185 (1996).
- [22] F. James, CERN Program Library Long Writeup D506. See <http://wwwasdoc.web.cern.ch/wwwasdoc/minuit/minmain.html>.
- [23] J. Pumplin *et al.*, Phys. Rev. **D65**, 014013 (2002).
- [24] For example, see <http://wwwasdoc.web.cern.ch/wwwasdoc/minuit/node33.html>, <http://www.library.cornell.edu/nr/bookpdf/f15-6.pdf>, <http://ccwww.kek.jp/pdg/2005/reviews/statrpp.pdf>. A different choice of $\Delta\chi^2$ is discussed in J. C. Collins and J. Pumplin, hep-ph/0105207.
- [25] L. W. Whitlow, S. Rock, A. Bodek, S. Dasu, and E. M. Riordan, Phys. Lett. **B250**, 193 (1990); L. W. Whitlow, report SLAC-0357 (1990); K. Abe *et al.*, Phys. Lett. **B452**, 194 (1999).
- [26] M. Glück, E. Reya, and A. Vogt, Eur. Phys. J. **C5**, 461 (1998).
- [27] European Muon Collaboration (EMC), J. Ashman *et al.*, Phys. Lett. **B206**, 364 (1988); Nucl. Phys. **B328**, 1 (1989).
- [28] Spin Muon Collaboration (SMC), B. Adeva *et al.*, Phys. Rev. **D58**, 112001 (1998).
- [29] SLAC-E130 collaboration, G. Baum *et al.*, Phys. Rev. Lett. **51**, 1135 (1983); E142 collaboration, P. L. Anthony *et al.*, Phys. Rev. **D54**, 6620 (1996); E143 collaboration, K. Abe *et al.*, Phys. Rev. **D58**, 112003 (1998); E154 collaboration, K. Abe *et al.*, Phys. Rev. Lett. **79**, 26 (1997); E155 collaboration, P. L. Anthony *et al.*, Phys. Lett. **B463**, 339 (1999); Phys. Lett. **B493**, 19 (2000).
- [30] HERMES collaboration, K. Ackerstaff *et al.*, Phys. Lett. **B404**, 383 (1997).
- [31] B. A. Kniehl, G. Kramer, and B. Pötter, Nucl. Phys. **B582**, 514 (2000).
- [32] W. Vogelsang, in BNL-52635, Proceedings of RIKEN BNL Research Center Workshop Vol 33, Spin Physics at RHIC in Year-1 and Beyond.

- [33] ZEUS Collaboration, S. Chekanov *et al.*, Eur. Phys. J. **C21**, 443 (2001).
- [34] See <http://casa.jlab.org/research/elic/elic.shtml> .
- [35] See http://www.phenix.bnl.gov/WWW/publish/abhay/Home_of_EIC/ .
- [36] M. Glück, E. Reya, M. Stratmann, and W. Vogelsang, Phys. Rev. **D63**, 094005 (2001).
- [37] J. Blümlein and H. Böttcher, Nucl. Phys. **B636**, 225 (2002).
- [38] E. Leader, A. V. Sidorov, and D. B. Stamenov, Phys. Rev. **D73**, 034023 (2006).
- [39] D. de Florian, G. A. Navarro, and R. Sassot, Phys. Rev. **D71**, 094018 (2005); C. Bourrely, J. Soffer, and F. Buccella, Eur. Phys. J. **C41**, 327 (2005).
- [40] T. Gehrmann and W. J. Stirling, Phys. Rev. **D53**, 6100 (1996); G. Altarelli, R. D. Ball, S. Forte, and G. Ridolfi, Nucl. Phys. **B496**, 337 (1997); Acta Phys. Pol. **B29**, 1145 (1998); L. E. Gordon, M. Goshtasbpour, and G. P. Ramsey, Phys. Rev. **D58**, 094017 (1998).
- [41] HERMES collaboration, A. Airapetian *et al.*, Phys. Rev. **D71**, 012003 (2005).
- [42] S. Kumano, Phys. Rep. **303**, 183 (1998); G. T. Garvey and J.-C. Peng, Prog. Part. Nucl. Phys. **47**, 203 (2001).
- [43] N. Saito, talk at the Particles and Nuclei International Conference Santa Fe, U.S.A, October 24-28, 2005.
- [44] S. J. Brodsky and I. Schmidt, Phys. Lett. **234**, 144 (1990).
- [45] One should note that the parameters are not determined within one percent accuracy.